



Charged vacancy in graphene: Interplay between Landau levels and atomic collapse resonancesJing Wang ^{1,2,3,4,*} Wen-Sheng Zhao ² Yue Hu,² R. N. Costa Filho,⁵ and François M. Peeters^{5,3,4,†}¹Key Laboratory of Micro-nano Sensing and IoT of Wenzhou, Wenzhou Institute of Hangzhou Dianzi University, Wenzhou 325038, China²School of Electronics and Information, Hangzhou Dianzi University, Hangzhou, Zhejiang Province 310038, China³Departement Fysica, Universiteit Antwerpen, Groenenborgerlaan 171, B-2020 Antwerpen, Belgium⁴NANOlaboratory Center of Excellence, University of Antwerp, Groenenborgerlaan 171, B-2020 Antwerpen, Belgium⁵Departamento de Física, Universidade Federal do Ceará, Caixa Postal 6030, Campus do Pici, 60455-760 Fortaleza, Ceará, Brazil

(Received 14 November 2023; accepted 5 February 2024; published 4 March 2024)

The interplay between a magnetic field and the Coulomb potential from a charged vacancy on the electron states in graphene is investigated within the tight-binding model. The Coulomb potential removes locally Landau level degeneracy, while the vacancy introduces a satellite level next to the normal Landau level. These satellite levels are found throughout the positive-energy region, but in the negative-energy region, they turn into atomic collapse resonances. Crossings between Landau levels with different angular quantum number m are found. Unlike the point impurity system in which an anticrossing occurs between Landau levels of the same m , in this work anticrossing is found between the normal Landau level and the vacancy-induced level. The atomic collapse resonance hybridizes with the Landau levels. The charge at which the lowest Landau level $m = -1$, $N = 1$ crosses $E = 0$ increases with enhancing magnetic field. A Landau level scaling anomaly occurs when the charge is larger than the critical charge $\beta \approx 0.6$ and this critical charge is independent of the magnetic field.

DOI: [10.1103/PhysRevB.109.104103](https://doi.org/10.1103/PhysRevB.109.104103)**I. INTRODUCTION**

Ever since the discovery of graphene, it has provided an effective medium to probe analogs and similarities of quantum electrodynamics (QED) phenomena [1]. The charge carriers in graphene are massless Dirac fermions with an effective “speed of light” $c \sim 10^6$ m/s [2]. For energies less than about 1 eV, the electron spectrum is conical with particular chirality of the electrons and holes around the high-symmetry K and K' points. Its unique electric properties allow the detection of the Klein paradox, which is a counterintuitive relativistic process [3]. Other QED phenomena, such as anomalous integer quantum Hall effect [4,5] and atomic collapse in artificial nuclei, were observed on graphene [6].

Atomic collapse is a fundamental quantum relativistic phenomenon [7]. It was predicted about 80 years ago, but turned out to be impossible to realize in real atoms. By assuming the nucleus to be a point charge, the collapse occurs whenever the charge exceeds the supercritical value $Z > Z_c = 137$ [8,9]. Taking into account the finite size of the nucleus, the condition becomes even more stringent, i.e., $Z_c = 170$. However, because of its large effective fine-structure constant, the critical charge in graphene is expected to be as low as $Z_c \sim 1-2$. By introducing charge impurities with $Z > 1$, atomic collapse has been realized experimentally in several different graphene systems [6,10,11]. Theoretically, similar phenomena have been intensively studied in both the subcritical and supercritical regimes. References [12–19] studied the atomic

collapse in graphene in a single charged impurity field. The extension to the case of two identical impurity charges was considered in Refs. [20–26]. The interaction between the two impurities splits the atomic collapse state into a pair of bonding and antibonding molecular collapse states. Furthermore, a new physical regime termed “frustrated supercritical collapse” was demonstrated [25]. When the “artificial nucleus” was realized with a charged vacancy in the graphene lattice, weak satellite states appeared beside the atomic (molecular) collapse resonances [10,26], which is a consequence of the discrete sublattice structure of graphene and the removal of the equivalence of the two sublattices.

It has been argued that a strong magnetic field can effectively reduce the value of the critical charge Z_c [27–31]. However, the situation in two dimensions is different and the effect of a magnetic field on a charged impurity in graphene leads to different conclusions. A theoretical study predicted that the magnetic field drives the critical charge to zero [32]. However, more recent investigations (some focused on an “exact” numerical solution) found that the magnetic field does not affect the value of the critical charge [19,33–36]. Recently, Eren and Güçlü investigated finite-size and external magnetic field effects on atomic collapse in a graphene quantum dot and concluded that the size of the quantum dot affects the value of the critical charge [37].

In previous works, a charged impurity was put on top of the graphene layer and it was concluded that (1) levels with the same orbital number m never cross each other, and (2) an anticrossing occurs between atomic collapse resonance energy levels [19,38]. Here we model the “artificial nuclei” by a charged vacancy as in the experiment of Ref. [10] and investigate the effect of a perpendicular magnetic field on the

*wangjing@hdu.edu.cn

†francois.peeters@uantwerpen.be

atomic collapse resonance states. In contrast to Refs. [19,38], the discrete nature of the graphene sublattice is retained in our approach and we will use the tight-binding model to calculate the electron states. How these new emerging states influence the crossing between Landau levels and collapse resonances is not clear and therefore triggers our interest and are investigated in this work. Whether the lifting of the sublattice symmetry due to the vacancy will induce any magnetic field dependence of the critical charge for atomic collapse will be critically examined.

The paper is organized as follows. In Sec. II, we present the model and the method used to obtain the relevant quantities. How the Landau levels cross atomic collapse resonant states in charged vacancy graphene is studied in Sec. III. The magnetic field dependence of the critical charge for atomic collapse is studied in Sec. IV. In Sec. V, we summarize our study.

II. MODEL

In order to model charged vacancies and to preserve effects due to the discrete lattice (i.e., to go beyond the continuum approach), we use the following tight-binding Hamiltonian:

$$\hat{H} = \sum_{\langle i,j \rangle} (t_{ij} \hat{a}_i^\dagger \hat{b}_j + \text{H.c.}) + \sum_i V_i \hat{a}_i^\dagger \hat{a}_i + \sum_j V_j \hat{b}_j^\dagger \hat{b}_j, \quad (1)$$

where \hat{a}_i (\hat{b}_j) represents the electron creation operator and \hat{a}_i^\dagger (\hat{b}_j^\dagger) is the annihilation operator of an electron at the sublattice A (B) at site i (j), and $t_{ij} = -2.8$ eV is the hopping strength between the nearest neighbors. The last two terms take into account the electrostatic potential $V_{i(j)}$ felt by the electron from the charged vacancy at site $i(j)$. The electric potential of the vacancy with effective charge $\beta = Z\alpha$ is $V(r) = -\hbar v_f \beta / r$, where Z is the value of the charge, α is the fine-structure constant of graphene, taking into account its environment, \hbar is the Planck constant divided by 2π , and v_f is the Fermi velocity. In order to simulate the finite size of the vacancy, a cutoff of the electron potential is introduced by replacing r with $r^* = 0.5$ nm when $r < 0.5$ nm. The value of r^* was determined in Ref. [10]. The charge on the vacancy can be tuned by firing voltage pulsed from an Scanning Tunneling Microscope (STM) tip on the vacancy [10]. To model a uniform magnetic field, we make use of Peierls' substitution and replace t_{ij} with $t_{ij} e^{i2\pi/\Phi_0 \int_i^j \vec{A}_{ij} d\vec{l}}$, where $\Phi_0 = h/e$ is the magnetic quantum, h is the Planck constant, and \vec{A}_{ij} is the magnetic vector potential along the path between sites i and j . The magnetic field is perpendicular to the graphene plane and the gauge is taken as $\vec{A}(x, y, z) = B(y, 0, 0)$. Electron-electron interaction is ignored because Ref. [37] indicates that the Hubbard parameter does not qualitatively change the results of atomic collapse, and the quantitative difference is small.

The eigenvalue problem with the Hamiltonian (1) is solved "numerically exact" on a hexagonal flake with armchair edges to avoid zigzag edges with zero-energy states. The charged impurity or vacancy is placed in the center of the flake. We take the hexagonal flake edge width of 200 nm, which is sufficiently large such that finite-size effects are negligible. Such a flake contains more than four million carbon atoms and we use the open-source tight-binding PYBINDING program to solve the problem numerically [39]. The package employs

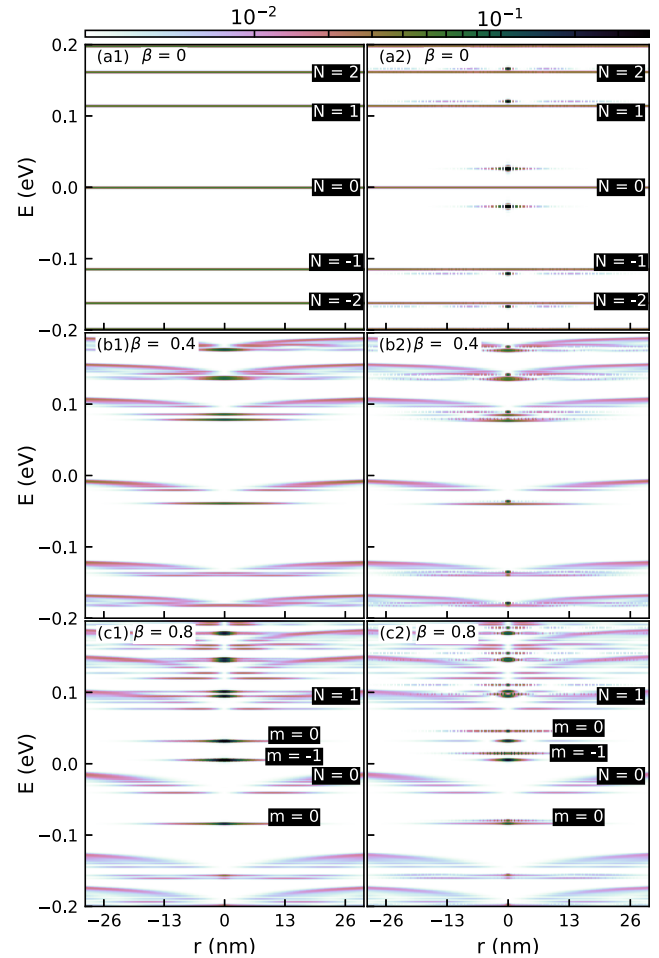


FIG. 1. Color map of the LDOS (in logarithmic scale) as a function of position and energy. (a1)–(c1) The results of a charged impurity above graphene is compared with (a2)–(c2) the results of a charged vacancy. Magnetic field strength is $B = 12$ T and the vacancy (charged impurity) is located at $r = 0$.

the kernel polynomial expansion to compute the local density of states (LDOS). An energy broadening of 1 meV is used to simulate effects due to disorder.

III. SINGLE VACANCY: EFFECT OF MAGNETIC FIELD

First, the space-energy map of the electronic states in the subcritical ($0 < \beta < 0.5$) and supercritical ($\beta > 0.5$) regimes is plotted in Fig. 1. Figures 1(a1)–1(c1) are for a point charged impurity which is put 5 nm above graphene and Figs. 1(a2)–1(c2) are for a charged vacancy system. Figure 1(a1) is for pristine graphene and Fig. 1(a2) is for a neutral vacancy in graphene. In the absence of an impurity, Landau levels are independent of the position. Notice that a vacancy introduces a satellite level beside each Landau level. These satellite levels are highly localized around the vacancy and their LDOS intensity rapidly decreases within one nanometer. In order to show the influence of the sublattice, the LDOS of the vacancy-induced satellite levels of Landau level $N = 0, 1,$ and 2 are plotted on different sublattices as a function of the radial distance r in Fig. 2 for $\beta = 0$. The vacancy is formed

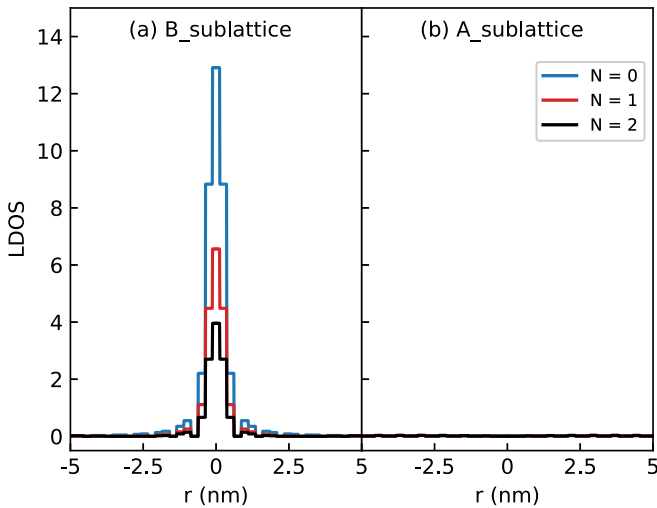


FIG. 2. The LDOS as a function of the radial distance r for the vacancy-induced level of Landau level $N = 0, 1$, and 2 in Fig. 1(a2). (a) The LDOS on the B sublattice and (b) the LDOS on the A sublattice. The results are for $\beta = 0$.

by removing an A sublattice atom, and we see that these vacancy-induced levels are localized on the B sublattice.

Adding charge, the Landau levels start to bend and split into sublevels for different orbital number m . Further increasing the charge, many more sublevels appear. In order to show this process clearly, the LDOS as a function of energy for several values of the distance from the impurity is shown in Fig. 3. The energy region was chosen to include only $N = 0$ and 1 Landau levels. At $\beta = 0.4$ in Fig. 3(b1), the peak labeled $m = 0$ belongs to $N = 0$; at $\beta = 0.8$ in Fig. 3(c1), the two peaks labeled $m = 0$ and -1 belong to $N = 1$. It is clear that the sublevels move down significantly in energy near the charge center. At the position slightly away from the charge center, new sublevels are observed but their downward movement is small. When the Landau levels are detected far away from the charge center, they tend not to split and their position is little affected by the charge. By replacing the point charge impurity with a charged vacancy, all of the above properties remain the same except that each level has a satellite level as shown in Figs. 3(a2)–3(c2). Due to the electron-hole symmetry, the $N = 0$ Landau level has two vacancy-induced satellite levels. In addition, these electron states have a high intensity close to the vacancy and disappear quickly away from it. In the following, we show only the results of a charged vacancy system and the LDOS will be computed at the vacancy.

The LDOS in Fig. 4 is plotted at the vacancy as a function of energy and charge. Without magnetic field, the atomic collapse states and vacancy-induced states are recognized from the high LDOS intensity in the negative-energy region. The naming of these LDOS resonances are the same as in Refs. [10,19] and are based on the spatial symmetry of their LDOS. VP represents the vacancy peak, R1 is the $1s$ atomic collapse state in atoms, R2 is the $2s$ state, and P1 is the $1p$ state. R1', R2', and P1' are their corresponding vacancy-induced satellite states. VP, R1', R2', and P1' are the consequence of the removal of a carbon atom resulting in the breaking of the sublattice symmetry and are absent in the

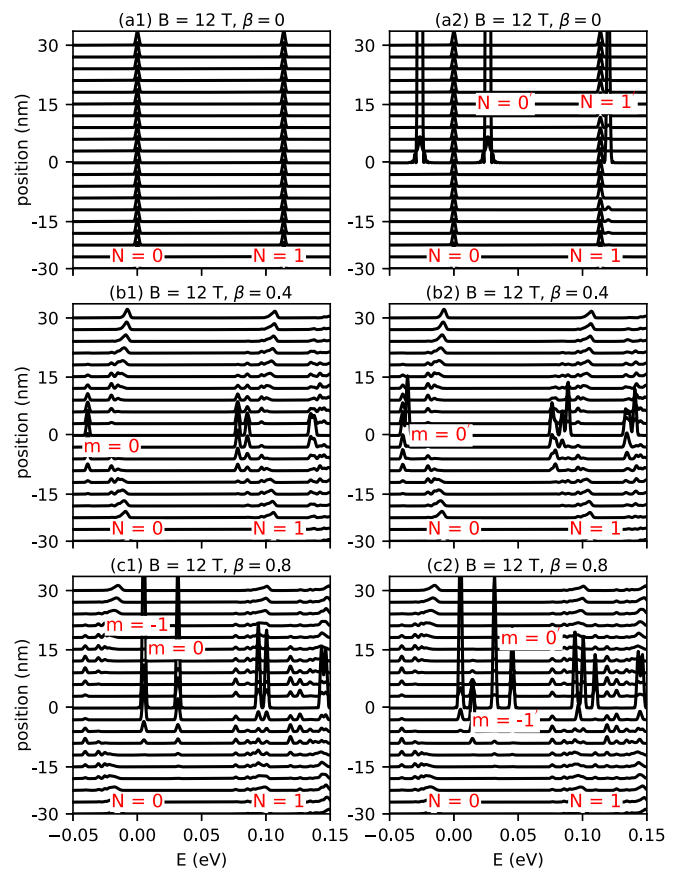


FIG. 3. The LDOS as a function of energy for different values of the distance from the charge. (a1)–(c1) A charged impurity 5 nm above the graphene plane and (a2)–(c2) for a charged vacancy.

case of a charged impurity system, as investigated in Ref. [19] within the continuum approach.

When a magnetic field is applied, Landau levels are clearly formed at low β . As the charge increases, Landau levels near the vacancy behave differently in the positive- and negative-energy region. Landau levels split into individual orbital states with different angular quantum number m in the positive-energy region. The Landau level $N = 1$ splits into orbital states $m = -1, m = -1', m = 0$, and $m = 0'$, followed by the

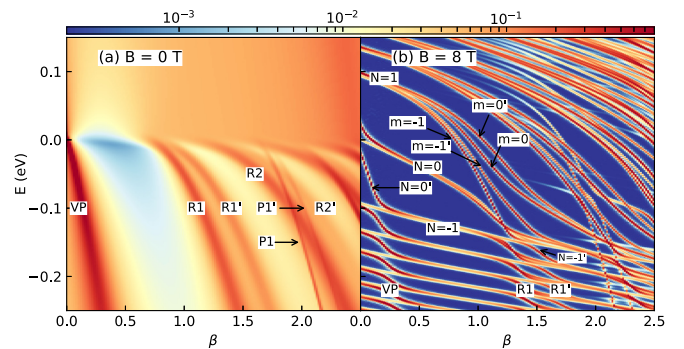


FIG. 4. Color map of the LDOS at the vacancy as a function of energy and charge β for (a) $B = 0$ and (b) $B = 8$ T. The vacancy is formed by removing an A sublattice atom.

splitting of higher Landau levels. The sublevels with accent ($'$) are vacancy-induced satellite levels. The annotation method of the splitting Landau level is consistent with Ref. [19] and is based on the spatial symmetry of the LDOS. Crossing and anticrossing are found between Landau levels of different quantum number as Landau levels drop into the negative-energy region. References [19,38] summarized the crossing law as level $N = 1, m = -1$ crosses level $N = 0, m = 0$ and is then repelled by level $N = -1, m = -1$ with the formation of an anticrossing following the atomic collapse resonance. This partially remains the same by replacing the point charge impurity with a charged vacancy in this work. Here, in addition, the level $N = 1, m = -1$ crosses level $N = 0, m = 0$, but is then repelled by the vacancy-induced satellite level $N = -1'$.

In addition to above phenomenon, Fig. 4(b) shows some new features due to the broken sublattice symmetry. At small charge, the value of the LDOS of the vacancy-induced electronic state is an order of magnitude larger than the value of the LDOS of normal Landau levels. It helps us to differentiate vacancy-induced levels from normal Landau levels by the color in Fig. 4(b). The vacancy-induced satellite levels (marked with superscript $'$) shift down one energy level through the VP resonance (which is independent of magnetic field) in the negative-energy region, e.g., level $N = 0'$ moves down to level $N = -1$. As the charge increases, but still less than the critical charge, those parallel levels are normal Landau levels. The interlevel spacing of these Landau levels is preserved until Landau levels cross the atomic collapse resonance. And the Landau levels shift down one energy level through the atomic collapse resonance. Meanwhile, the vacancy-induced levels reappear (e.g., level $N = -1'$) after Landau levels cross R1 resonance and they merge into the lower Landau level through R1' resonance. This process repeats and higher orbital states become involved with increase of charge and $|E|$.

Another interesting feature in Fig. 4(b) needs to be discussed. The vacancy-induced satellite levels exist throughout the positive-energy region, but in the negative-energy region, these levels merge into the normal Landau levels in the region where the vacancy-induced resonances do not exist. Thus, the separation distance between the normal Landau level and its satellite level first increases, then decreases with increasing charge β . In the Supplemental Material (SM) [40], we show the LDOS calculated on both sublattices separately. They exhibit an out-of-phase oscillation which is similar to what was found in Ref. [10].

IV. CRITICAL CHARGE FOR ATOMIC COLLAPSE

Next, the LDOS of electronic states are investigated as a function of magnetic field and energy. The results are plotted in Fig. 5 for $\beta = 0, 0.4, 0.8, 1.2$, and 2.0 . Landau levels show \sqrt{B} behavior when the charge is smaller than some critical charge, as shown in Figs. 5(a) and 5(b). As the charge increases beyond some critical charge, the lowest Landau level $m = -1, N = 1$ crosses $E = 0$ and no longer shows the \sqrt{B} scaling, as shown in Fig. 5(c). At small \sqrt{B} , an apparent feature is the atomic collapse state that is formed. The $m = -1, N = 1$ Landau level (LL) crosses $E = 0$ and is included

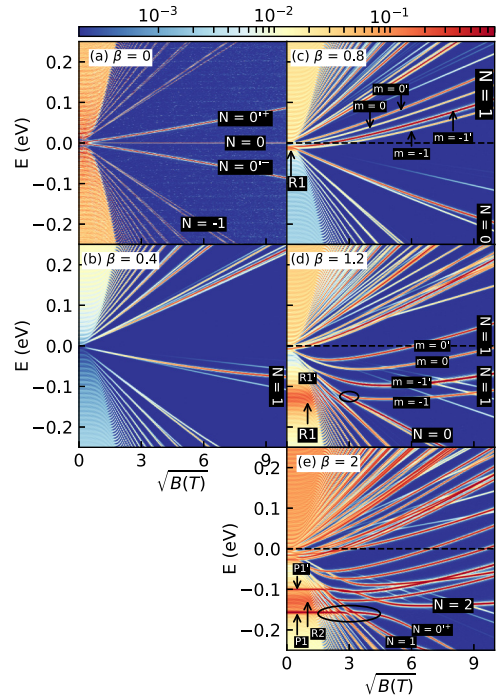


FIG. 5. Color map of LDOS taken at the vacancy as a function of energy and \sqrt{B} for several charges. (a) $\beta = 0$, (b) $\beta = 0.4$, (c) $\beta = 0.8$, (d) $\beta = 1.2$, and (e) $\beta = 2$. The horizontal black dotted line is at $E = 0$.

in the atomic collapse resonance. Thus, the atomic collapse resonance hybridizes with the Landau level. But for larger \sqrt{B} in Fig. 5(c), the $m = -1, N = 1$ LL and the atomic collapse resonance locate at different energies. Further increasing the charge, the R1 atomic collapse resonance moves downward and hybridizes again with $m = -1, N = 1$ LL at larger \sqrt{B} in Fig. 5(d). Thus, as the magnetic field increases, the charge at which the $m = -1, N = 1$ LL crosses $E = 0$ increases. In Refs. [32,37], the crossing of this LL with $E = 0$ was used to determine the value of the critical charge. In Fig. 6, this charge is plotted as a function of magnetic field and fitted to $\beta = 103 * B^{1/3} + 0.6$. According to this criterion, the critical charge increases with B .

According to the discussion of Fig. 4, we know that the crossing and anticrossing between Landau levels only occur in the atomic collapse resonance region. This is reconfirmed by Figs. 5(d) and 5(e). The crossing between Landau level $N = 1, m = -1$ and Landau level $N = 0, m = 0$ is highlighted by the circle in Fig. 5(d). As the charge increases, the R1 atomic collapse resonance falls to a lower energy, meanwhile R2 and P1 atomic collapse appears as shown in Fig. 5(e). Crossing and anticrossing between higher-order Landau levels are pointed out by the circle in Fig. 5(e). These crossing and anticrossing points are located at the same energies as the atomic collapse resonances. Previously, the absence of \sqrt{B} scaling of the LL was used to determine the critical charge for atomic collapse [19]. The energy of the Landau level N can be written as

$$E_N(B) = \pm v_F \sqrt{2|N|\hbar} \sqrt{B} = \pm v_N \sqrt{B}, \quad (2)$$

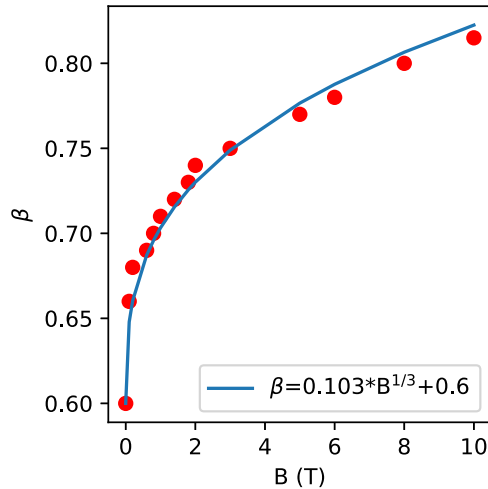


FIG. 6. The charge at which the Landau level $N = 1$, $m = -1$ crosses zero energy vs magnetic field. The numerical results are fitted to $\beta = 0.103 * B^{1/3} + 0.6$.

where $\pm\nu_N$ is the level scaling prefactor. When β is 0, $\partial\nu_N/\partial B = 0$ and Eq. (2) is satisfied. On the other hand, $\partial\nu_N/\partial B \neq 0$ means the level has a scaling anomaly. We use the LDOS data to calculate the derivative $\partial\nu_1/\partial B$ for Landau level $N = 1$, $m = -1$ and present the results in Fig. 7. The derivative is almost a constant and close to 0 for $\beta \leq 0.6$, independent of the magnetic field. A constant derivative implies $E_N(B) = \pm(\nu_N\sqrt{B} + \gamma_N B^{3/2})$ with γ small, and the \sqrt{B} scaling of the LLs is, to a large extent, satisfied. For $\beta > 0.6$, there is a significant nonlinear enlargement at small values of the magnetic field. The scaling anomaly is mainly a function of energy and, therefore, we plot $\partial\nu_1/\partial B$ as a function of energy in Fig. 7(b). Note that for $E < 0$, $\partial\nu_1/\partial B = 0$ when $\beta \leq 0.6$, and we have perfect \sqrt{B} scaling. Once β increases beyond 0.6, the derivative is also nonzero for $E < 0$. Without magnetic field, the critical charge in a single impurity system was previously determined in the continuum limit to be ≈ 0.5 . Here we found a slightly larger value of ≈ 0.6 , but the most important conclusion is that the magnetic field does not affect the value of the critical charge.

V. CONCLUSION

In this work, we studied how the electronic states of graphene are modified in the presence of a charged vacancy and a perpendicular magnetic field. A charged vacancy causes Landau levels to split into sublevels with different quantum number m and introduces a satellite level next to each

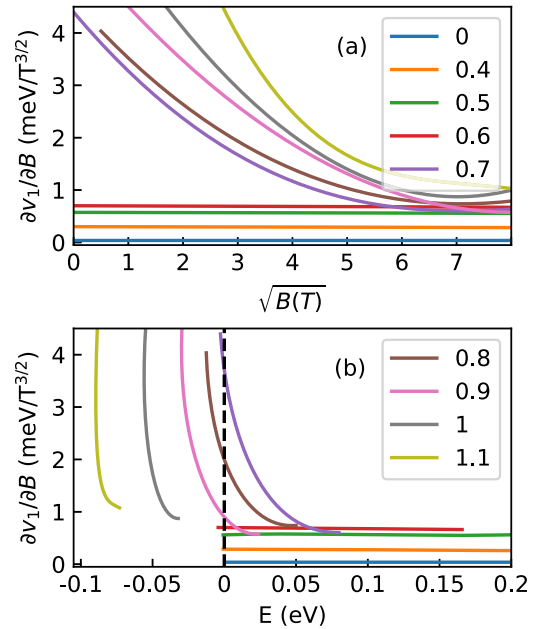


FIG. 7. (a) The derivative of the scaling ν_1 for different values of the charge β for Landau level $N = 1$, $m = -1$. (b) Same derivative, but presented as a function of energy instead of the magnetic field.

normal Landau level. Crossings and anticrossings are formed between Landau levels of different quantum number and the Landau level repulsion occurs between normal Landau level and vacancy-induced level. The atomic collapse resonance hybridizes with Landau levels and the magnetic field increases the charge at which the lowest Landau level $m = -1$, $N = 1$ crosses $E = 0$. This $E = 0$ crossing criterium will result in different critical charge for different energy levels. This is different for the scaling anomaly criterium, which results in a critical charge independent of the chosen energy level and independent of the magnetic field. Therefore, the scaling anomaly argument is more fundamental and is therefore considered to be the correct criterium. As compared to previous results for the continuum Dirac-Kepler problem, we find a slightly larger value of $\beta_c \approx 0.6$ for the critical charge for atomic collapse.

ACKNOWLEDGMENTS

This work was supported by the National Natural Science Foundation of China (Grant No. 62004053), Wenzhou Science & Technology Bureau Project (Grant No. L2023007), and Provice Natural Science Foundation of China (Grant No. LY19F040006).

- [1] K. S. Novoselov, A. K. Geim, S. V. Morozov, D. Jiang, Y. Zhang, S. V. Dubonos, I. V. Grigorieva, and A. A. Firsov, *Science* **306**, 666 (2004).
- [2] A. H. Castro Neto, F. Guinea, N. M. R. Peres, K. S. Novoselov, and A. K. Geim, *Rev. Mod. Phys.* **81**, 109 (2009).
- [3] M. I. Katsnelson, K. S. Novoselov, and A. K. Geim, *Nat. Phys.* **2**, 620 (2006).

- [4] K. S. Novoselov, A. K. Geim, S. V. Morozov, D. Jiang, M. I. Katsnelson, I. V. Grigorieva, S. V. Dubonos, and A. A. Firsov, *Nature (London)* **438**, 197 (2005).
- [5] Y. Zhang, Y.-W. Tan, H. L. Stormer, and P. Kim, *Nature (London)* **438**, 201 (2005).
- [6] Y. Wang, D. Wong, A. V. Shytov, V. W. Brar, S. Choi, Q. Wu, H.-Z. Tsai, W. Regan, A. Zettl, R. K. Kawakami, S. G.

- Louie, L. S. Levitov, and M. F. Crommie, *Science* **340**, 734 (2013).
- [7] J. Reinhardt and W. Greiner, *Rep. Prog. Phys.* **40**, 219 (1977).
- [8] J. Schweppe, A. Gruppe, K. Bethge, H. Bokemeyer, T. Cowan, H. Folger, J. S. Greenberg, H. Grein, S. Ito, R. Schule, D. Schwalm, K. E. Stiebing, N. Trautmann, P. Vincent, and M. Waldschmidt, *Phys. Rev. Lett.* **51**, 2261 (1983).
- [9] T. Cowan, H. Backe, M. Begemann, K. Bethge, H. Bokemeyer, H. Folger, J. S. Greenberg, H. Grein, A. Gruppe, Y. Kido, M. Klüver, D. Schwalm, J. Schweppe, K. E. Stiebing, N. Trautmann, and P. Vincent, *Phys. Rev. Lett.* **54**, 1761 (1985).
- [10] J. Mao, Y. Jiang, D. Moldovan, G. Li, K. Watanabe, T. Taniguchi, M. R. Masir, F. M. Peeters, and E. Y. Andrei, *Nat. Phys.* **12**, 545 (2016).
- [11] Y. Jiang, J. Mao, D. Moldovan, M. R. Masir, G. Li, K. Watanabe, T. Taniguchi, F. M. Peeters, and E. Y. Andrei, *Nat. Nanotechnol.* **12**, 1045 (2017).
- [12] A. V. Shytov, M. I. Katsnelson, and L. S. Levitov, *Phys. Rev. Lett.* **99**, 236801 (2007).
- [13] V. M. Pereira, J. Nilsson, and A. H. Castro Neto, *Phys. Rev. Lett.* **99**, 166802 (2007).
- [14] M. M. Fogler, D. S. Novikov, and B. I. Shklovskii, *Phys. Rev. B* **76**, 233402 (2007).
- [15] I. S. Terekhov, A. I. Milstein, V. N. Kotov, and O. P. Sushkov, *Phys. Rev. Lett.* **100**, 076803 (2008).
- [16] A. H. Castro Neto, V. N. Kotov, J. Nilsson, V. M. Pereira, N. M. R. Peres, and B. Uchoa, *Solid State Commun.* **149**, 1094 (2009).
- [17] D. S. Novikov, *Phys. Rev. B* **76**, 245435 (2007).
- [18] V. N. Kotov, B. Uchoa, V. M. Pereira, F. Guinea, and A. H. Castro Neto, *Rev. Mod. Phys.* **84**, 1067 (2012).
- [19] D. Moldovan, M. R. Masir, and F. M. Peeters, *2D Mater.* **5**, 015017 (2017).
- [20] R. V. Pottelberge, D. Moldovan, S. P. Milovanović, and F. M. Peeters, *2D Mater.* **6**, 045047 (2019).
- [21] A. De Martino, D. Klöpfer, D. Matrasulov, and R. Egger, *Phys. Rev. Lett.* **112**, 186603 (2014).
- [22] D. Klöpfer, A. D. Martino, D. U. Matrasulov, and R. Egger, *Eur. Phys. J. B* **87**, 187 (2014).
- [23] E. V. Gorbar, V. P. Gusynin, and O. O. Sobol, *Phys. Rev. B* **92**, 235417 (2015).
- [24] R. Van Pottelberge, B. Van Duppen, and F. M. Peeters, *Phys. Rev. B* **98**, 165420 (2018).
- [25] J. Lu, H.-Z. Tsai, A. N. Tatan, S. Wickenburg, A. A. Omrani, D. Wong, A. Riss, E. Piatti, K. Watanabe, T. Taniguchi, A. Zettl, V. M. Pereira, and M. F. Crommie, *Nat. Commun.* **10**, 477 (2019).
- [26] J. Wang, M. Anđelković, G. Wang, and F. M. Peeters, *Phys. Rev. B* **102**, 064108 (2020).
- [27] V. P. Krainov and S. I. Zakharov, *Sov. Phys.-JETP* **37**, 983 (1973).
- [28] V. N. Oraevskii, A. I. Rex, and V. B. Semikoz, *Zh. Eksp. Teor. Fiz.* **72**, 820 (1977) [*Sov. Phys.-JETP* **45**, 428 (1977)].
- [29] B. M. Karakov and V. S. Popov, *J. Expt. Theor. Phys.* **97**, 890 (2003).
- [30] M. I. Vysotskii and S. I. Godunov, *Phys. Usp.* **57**, 194 (2014).
- [31] E. V. Gorbar, V. P. Gusynin, and O. O. Sobol, *Low Temp. Phys.* **44**, 371 (2018).
- [32] O. V. Gamayun, E. V. Gorbar, and V. P. Gusynin, *Phys. Rev. B* **83**, 235104 (2011).
- [33] D. Valenzuela, S. Hernández-Ortiz, M. Loewe, and A. Raya, *J. Phys. A: Math. Theor.* **49**, 495302 (2016).
- [34] Y. Zhang, Y. Barlas, and K. Yang, *Phys. Rev. B* **85**, 165423 (2012).
- [35] T. Maier and H. Siedentop, *J. Math. Phys.* **53**, 095207 (2012).
- [36] S. C. Kim and S.-R. Eric Yang, *Ann. Phys.* **347**, 21 (2014).
- [37] I. Eren and A. D. Güçlü, *Solid State Commun.* **351**, 114763 (2022).
- [38] O. O. Sobol, P. K. Pyatkovskiy, E. V. Gorbar, and V. P. Gusynin, *Phys. Rev. B* **94**, 115409 (2016).
- [39] D. Moldovan, M. Anđelković, and F. M. Peeters, Pybinding V0.9.4: A Python Package For Tight-Binding Calculations, <https://docs.pybinding.site/en/stable/>.
- [40] See Supplemental Material at <http://link.aps.org/supplemental/10.1103/PhysRevB.109.104103> for the sublattice contribution to LDOS and the spatial LDOS of Landau levels.